Supplementary Information

First-Principles Investigation of Lithium Ion First-In-First-Out Behavior during Delithiation and Lithiation Processes in Li2MnO3 Lithium-Rich Cathode Material

Yuyang Chen,* Yuxin Wei, Yunsong Zhang and Rui Li

New Energy Storage Technology and Vocational Skills Innovation Research Center, Beijing Polytechnic College, Beijing 100042, China

Fig. S1 and Fig. S2 show the comparison of voltage curves and electronic structures of Li_2MnO_3 based on the SCAN+rVV10 and PBE+D3 exchange–correlation functionals. The voltage profiles obtained using the SCAN+rVV10 and PBE+D3 exchange–correlation functionals show that SCAN+rVV10 predicts a lower initial delithiation voltage, which is also closer to the experimental value. In the later stages of delithiation, SCAN+rVV10 yields a slightly higher voltage window compared with PBE+D3. Overall, the higher-level SCAN+rVV10 functional produces a larger difference between the initial voltage and the voltage window, resulting in a description that agrees more closely with experimental observations and offers improved accuracy.

The electronic-structure results show that both functionals exhibit consistent overall trends in the density of states of oxygen and manganese. However, the band gap calculated using SCAN+rVV10 is approximately 1.4 eV, whereas PBE+D3 yields a slightly smaller value of around 1.1 eV. Since the GGA-based PBE functional is known to underestimate band gaps, applying a +U correction can partially mitigate this deviation. In summary, the higher-level SCAN+rVV10 functional provides more accurate predictions of both the voltage profiles and electronic structure, while the PBE+D3 method with a +U correction offers a computationally more efficient approach that still provides reasonable and meaningful interpretations for the system studied in this work.

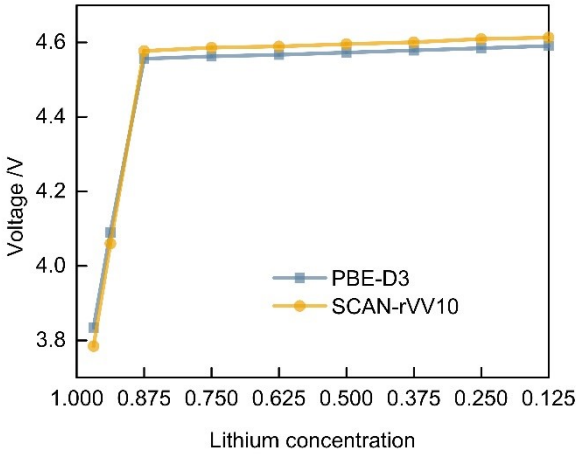

Fig. S1 Simulated voltage curves of Li_2MnO_3 based on the SCAN+rVV10 and PBE+D3 pseudopotentials.

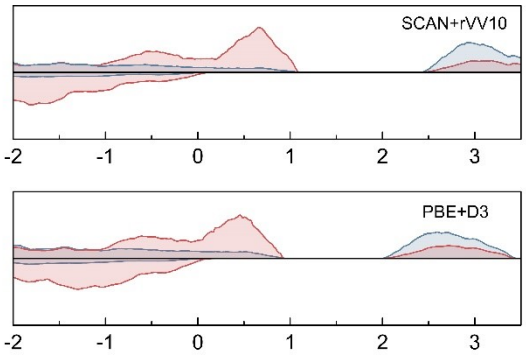

Fig. S2 Partial density of states of Mn and O from 75% lithium structure based on the SCAN+rVV10 and PBE+D3 pseudopotentials.

Fig. S3 to Fig. S32 show thirty computationally stable structures with different lithium contents and distributions. The CIF files obtained from VASP calculations are provided in the attachment.

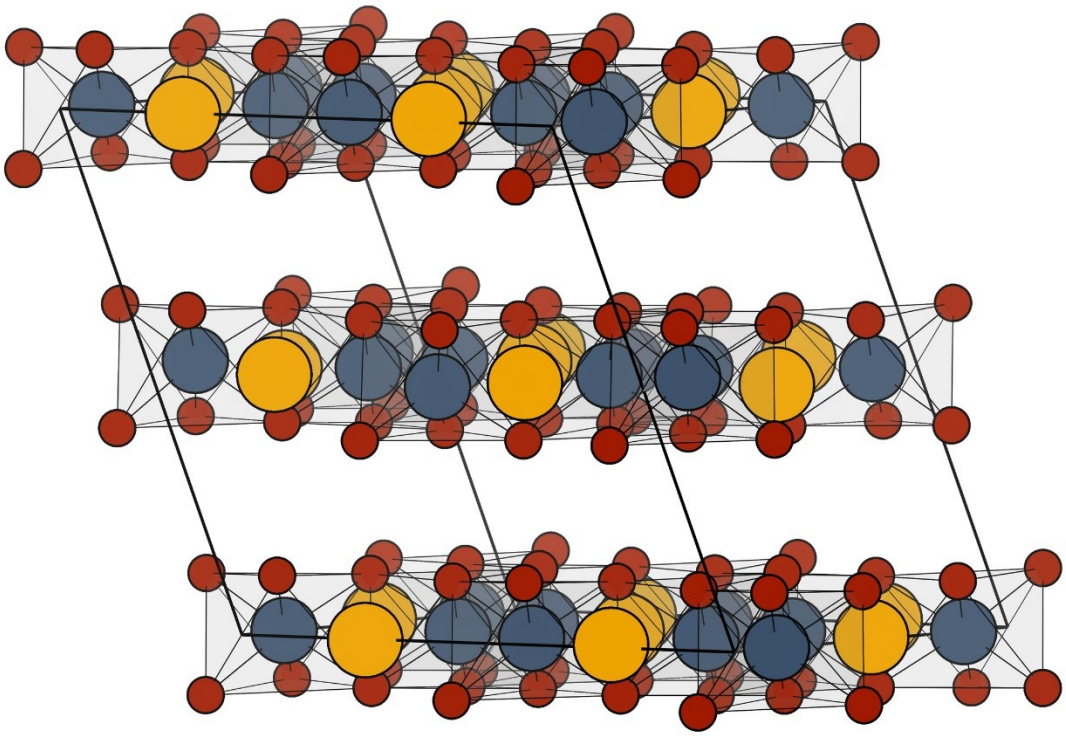

Fig S3 Calculated structure of Li_0(Li-layer)Li_8(Mn-layer)$Mn_{16}O_{48}$

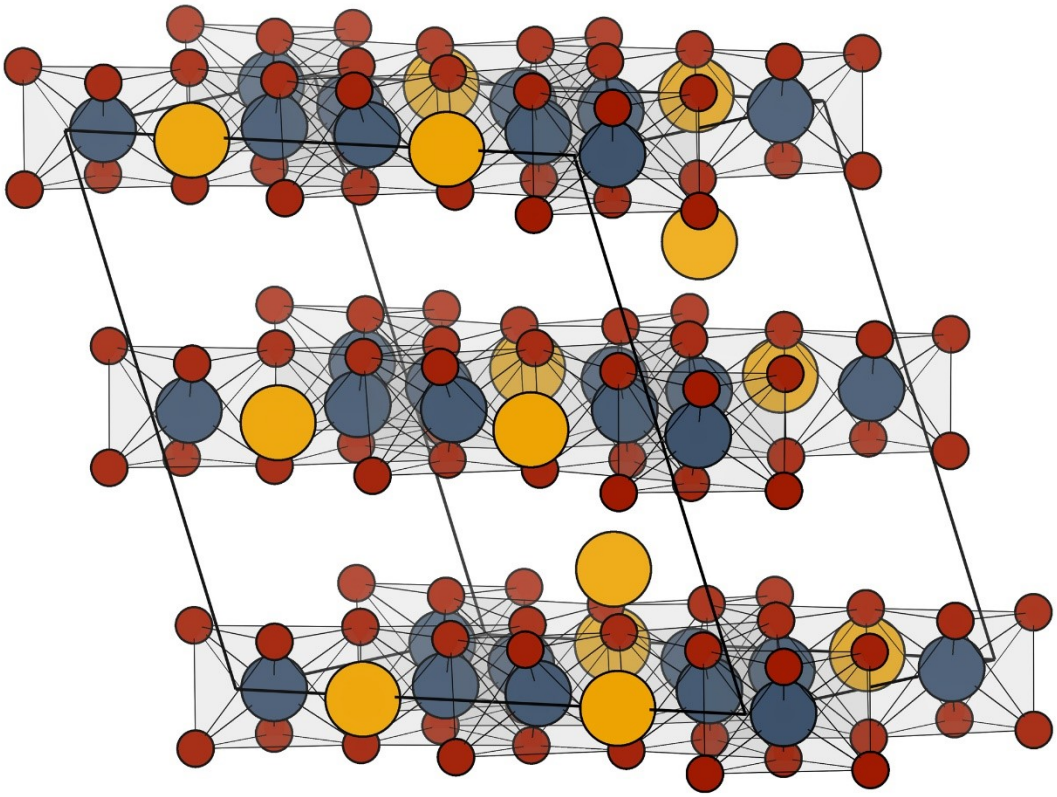

Fig S4 Calculated structure of Li_2(Li-layer)Li_6(Mn-layer)$Mn_{16}O_{48}$

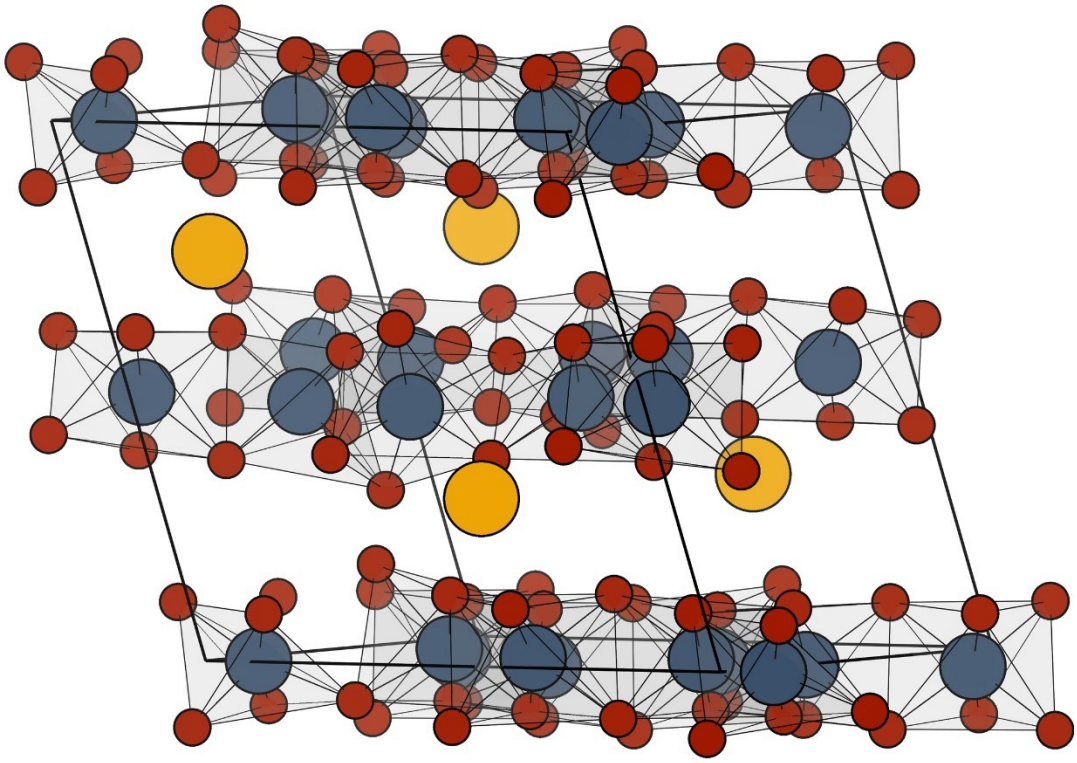

Fig S5 Calculated structure of Li_4(Li-layer)Li_0(Mn-layer)$Mn_{16}O_{48}$

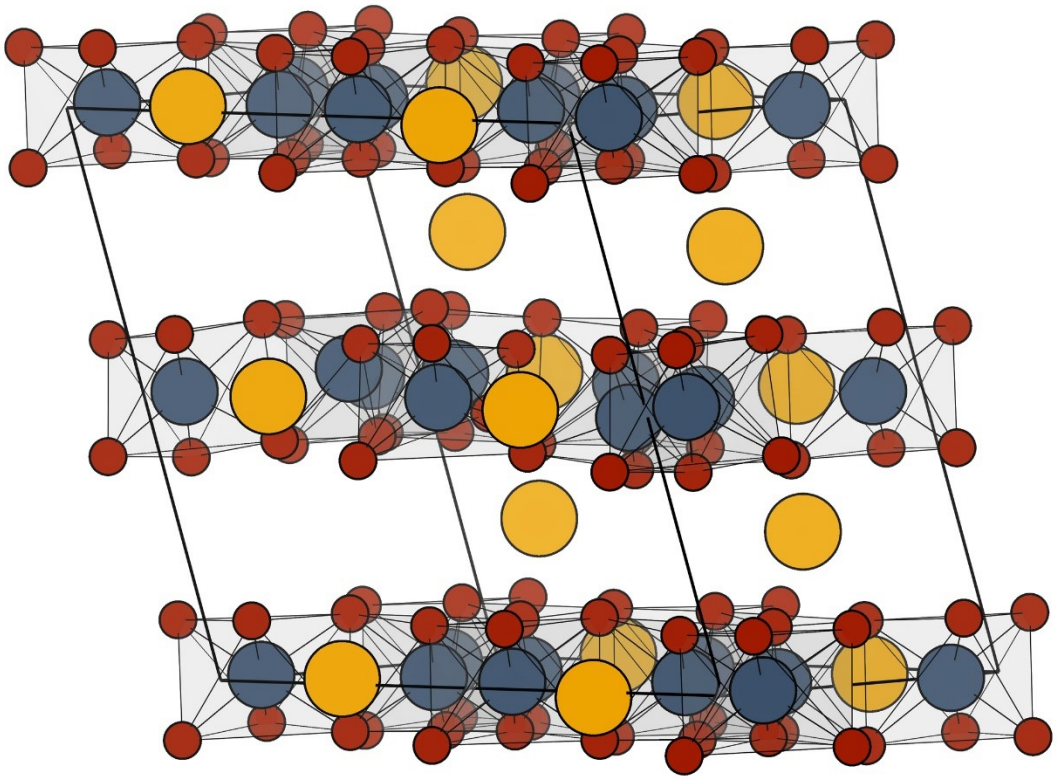

Fig S6 Calculated structure of Li_4(Li-layer)Li_4(Mn-layer)$Mn_{16}O_{48}$

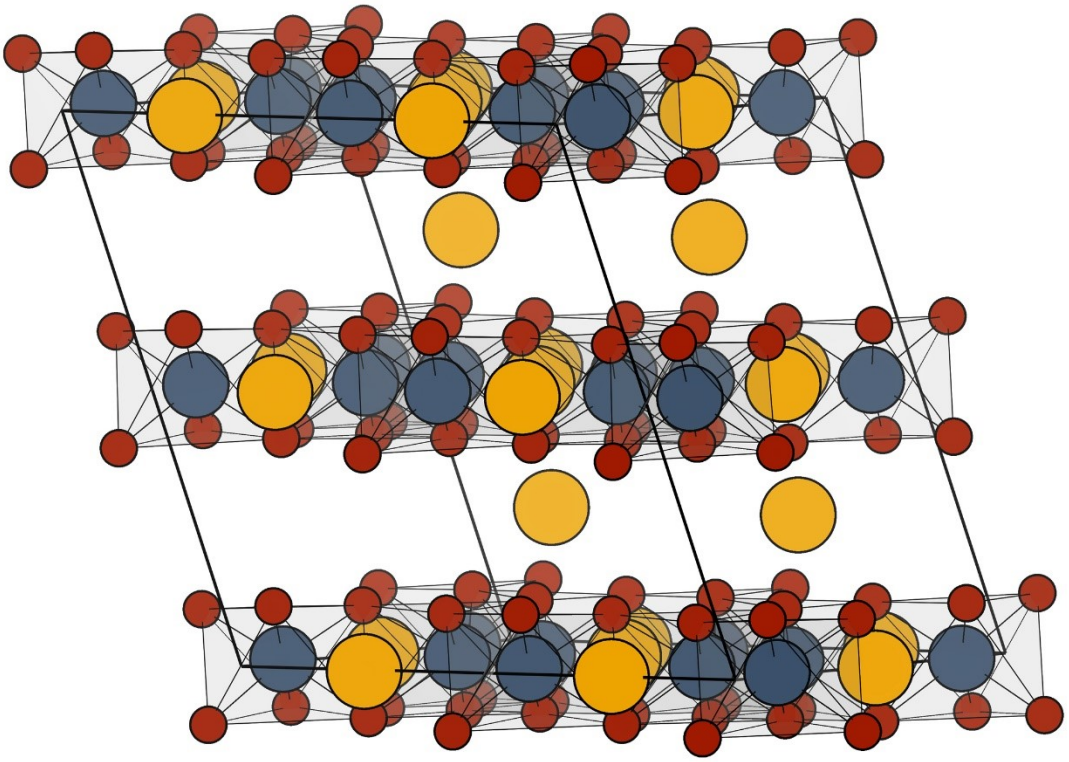

Fig S7 Calculated structure of Li_4(Li-layer)Li_8(Mn-layer)$Mn_{16}O_{48}$

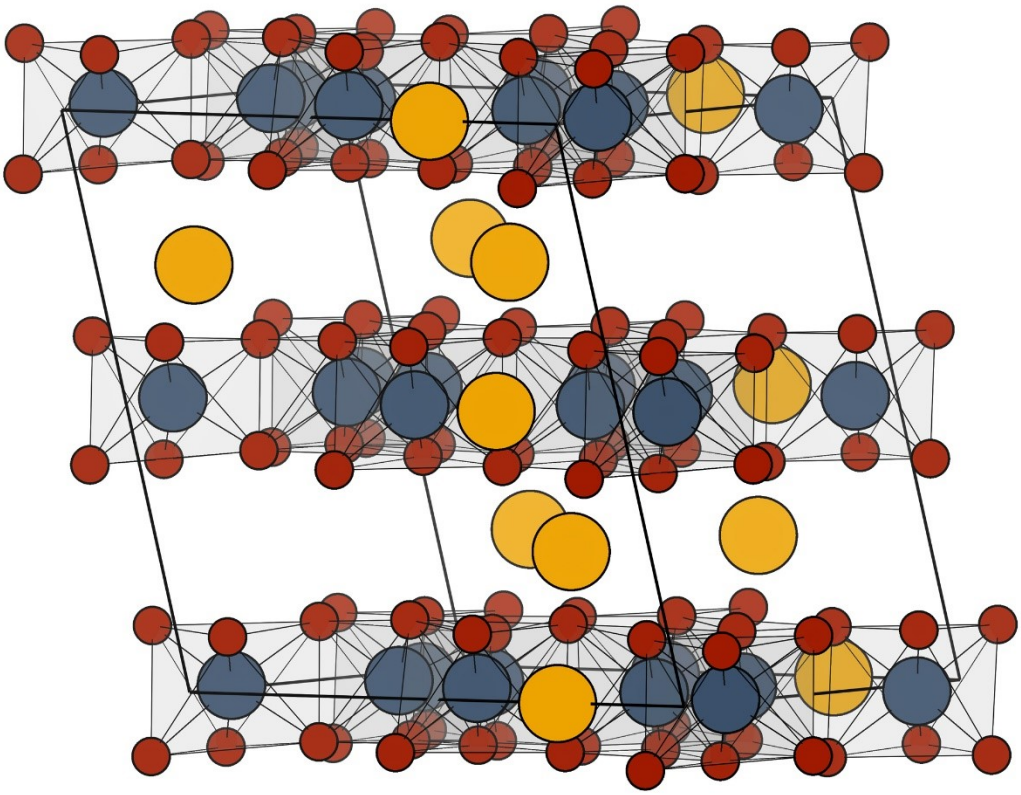

Fig S8 Calculated structure of Li_6(Li-layer)Li_2(Mn-layer)$Mn_{16}O_{48}$

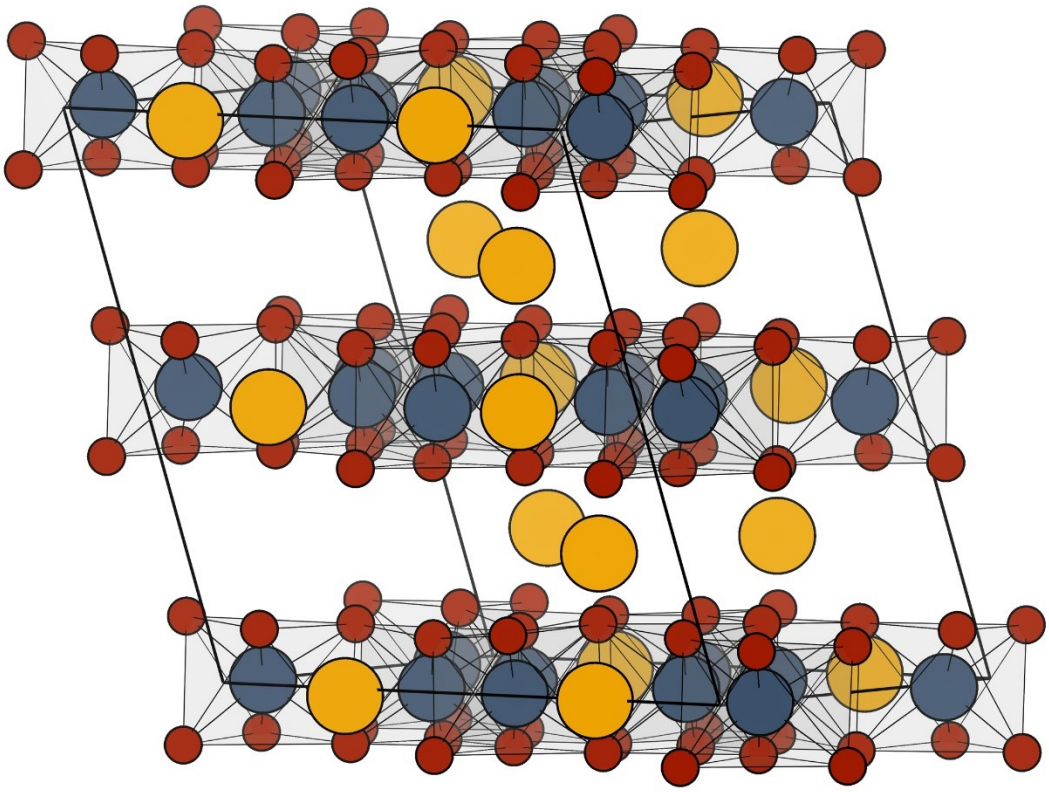

Fig S9 Calculated structure of Li_6(Li-layer)Li_6(Mn-layer)$Mn_{16}O_{48}$

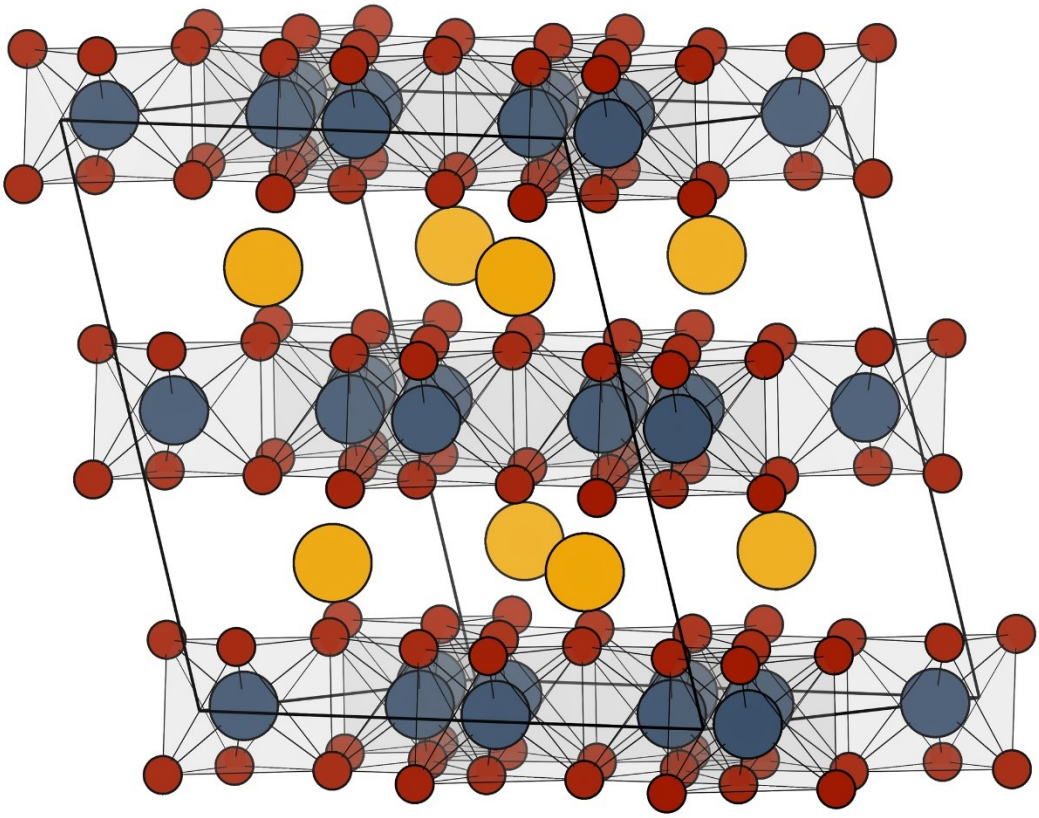

Fig S10 Calculated structure of Li_8(Li-layer)Li_0(Mn-layer)$Mn_{16}O_{48}$

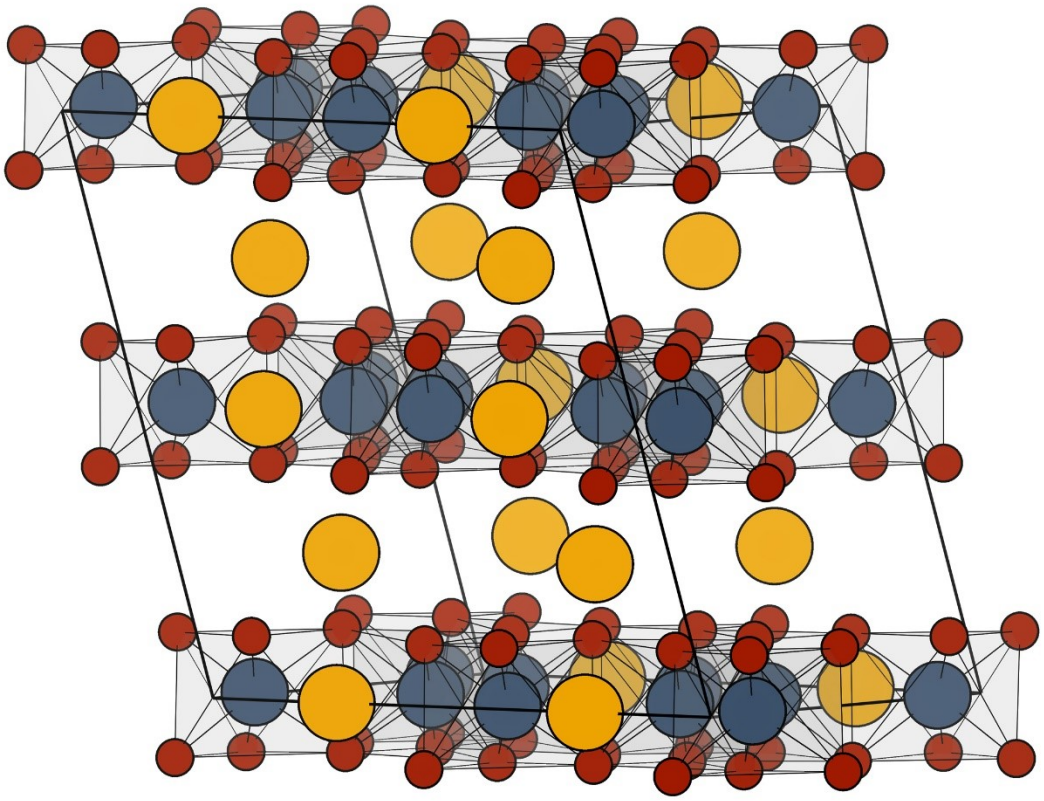

Fig S11 Calculated structure of Li_8(Li-layer)Li_4(Mn-layer)$Mn_{16}O_{48}$

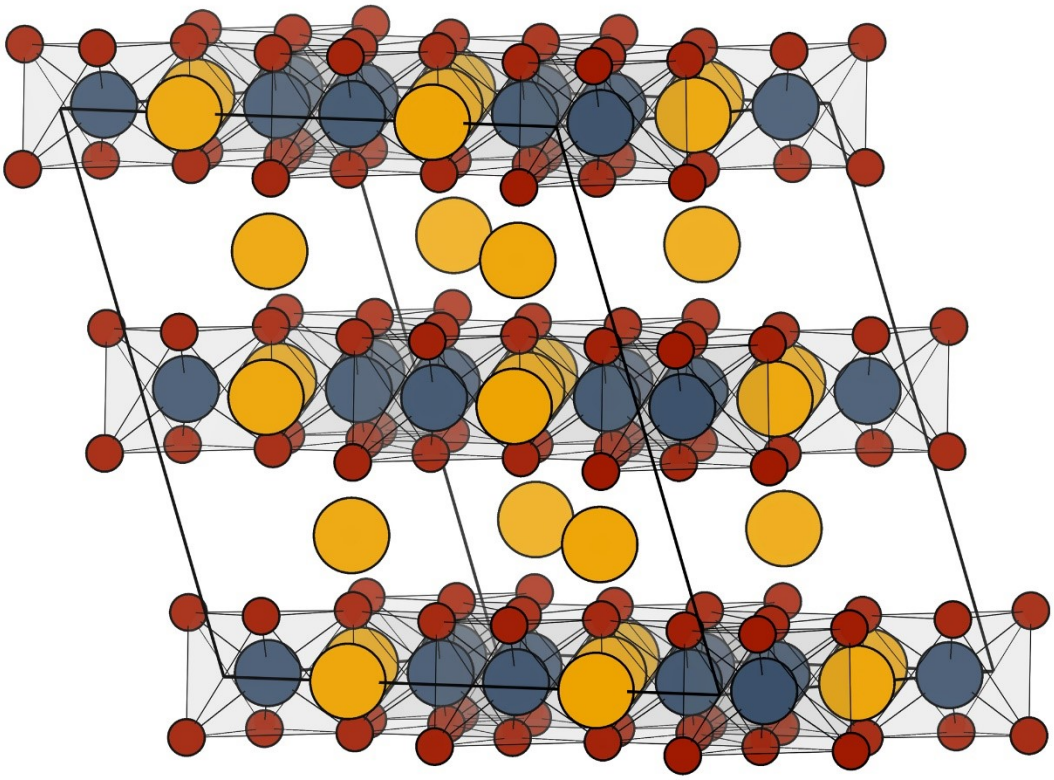

Fig S12 Calculated structure of Li_8(Li-layer)Li_8(Mn-layer)$Mn_{16}O_{48}$

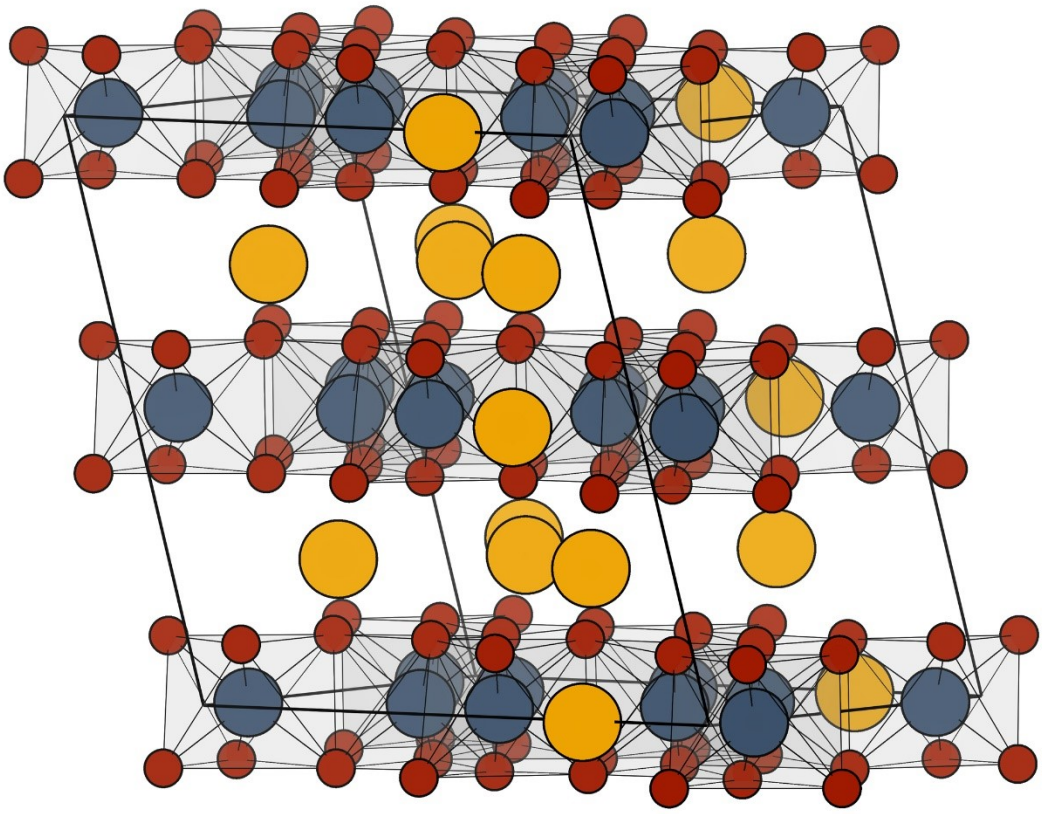

Fig S13 Calculated structure of Li_{10}(Li-layer)Li_2(Mn-layer)$Mn_{16}O_{48}$

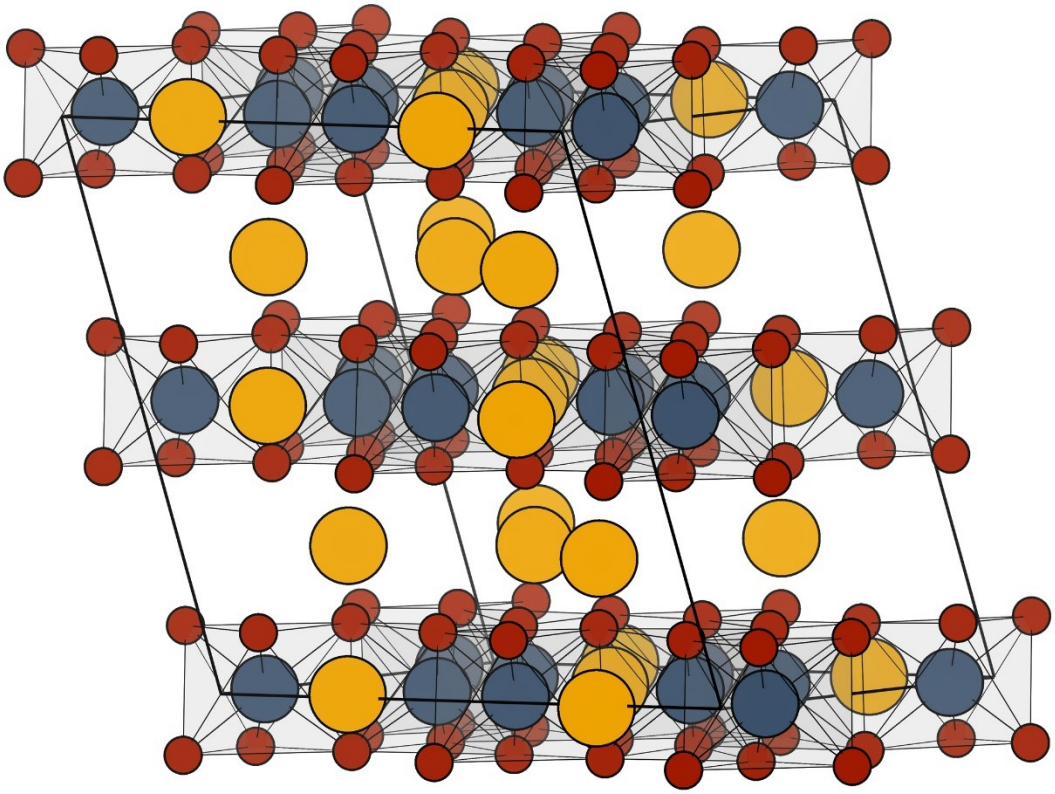

Fig S14 Calculated structure of Li_{10}(Li-layer)Li_6(Mn-layer)$Mn_{16}O_{48}$

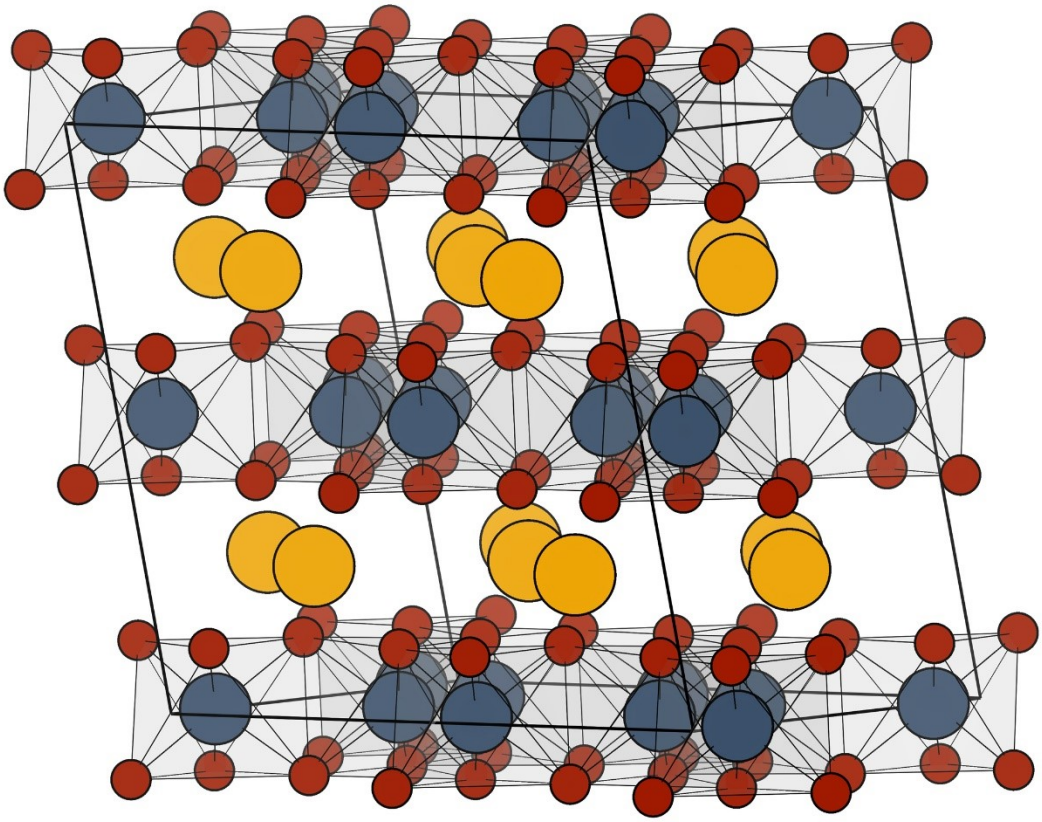

Fig S15 Calculated structure of Li_{12}(Li-layer)Li_0(Mn-layer)$Mn_{16}O_{48}$

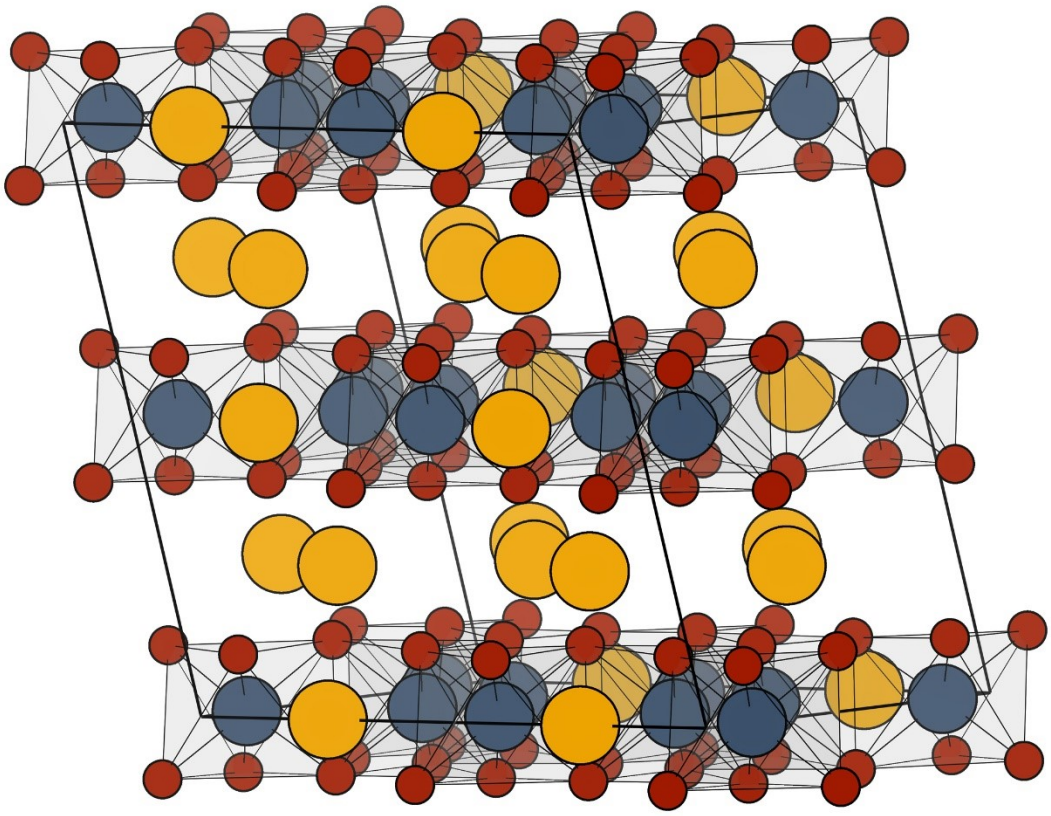

Fig S16 Calculated structure of Li_{12}(Li-layer)Li_4(Mn-layer)$Mn_{16}O_{48}$

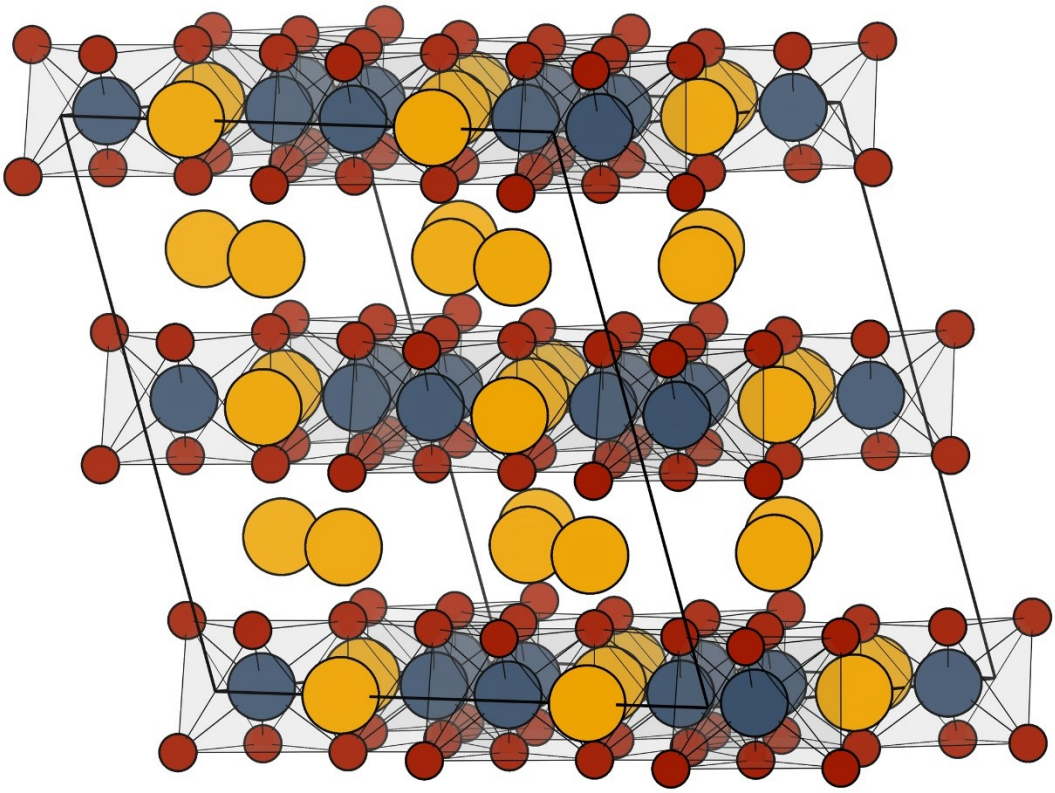

Fig S17 Calculated structure of Li_{12}(Li-layer)Li_8(Mn-layer)$Mn_{16}O_{48}$

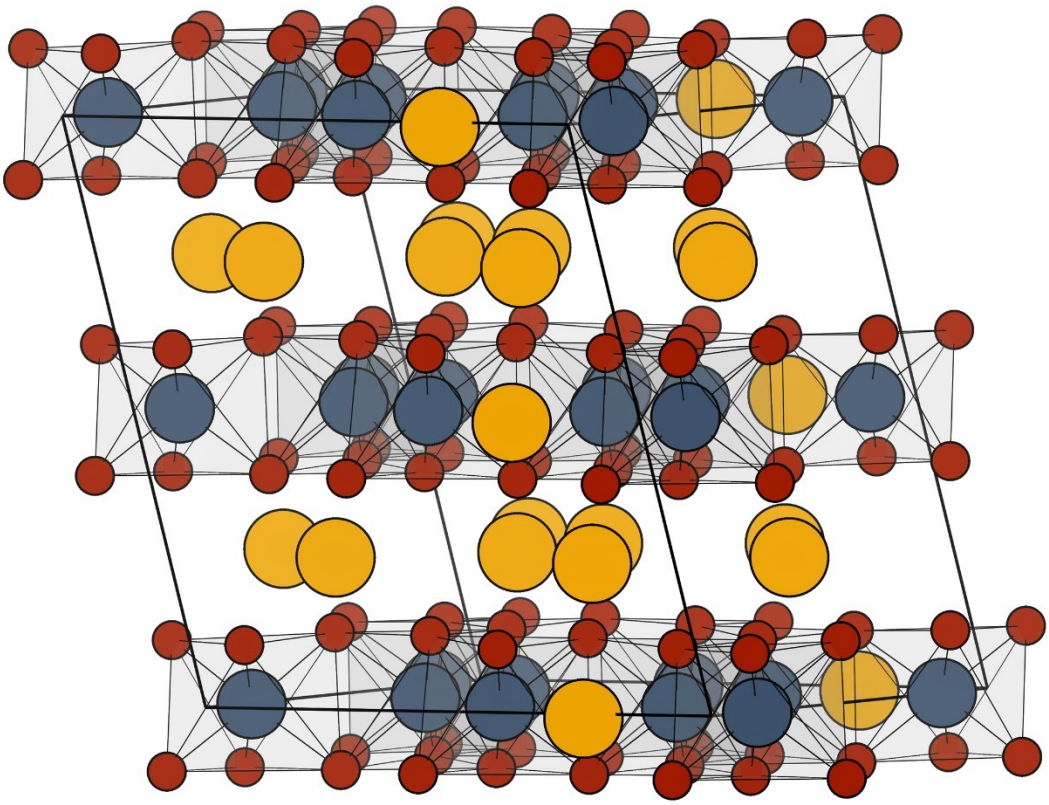

Fig S18 Calculated structure of Li_{14}(Li-layer)Li_2(Mn-layer)$Mn_{16}O_{48}$

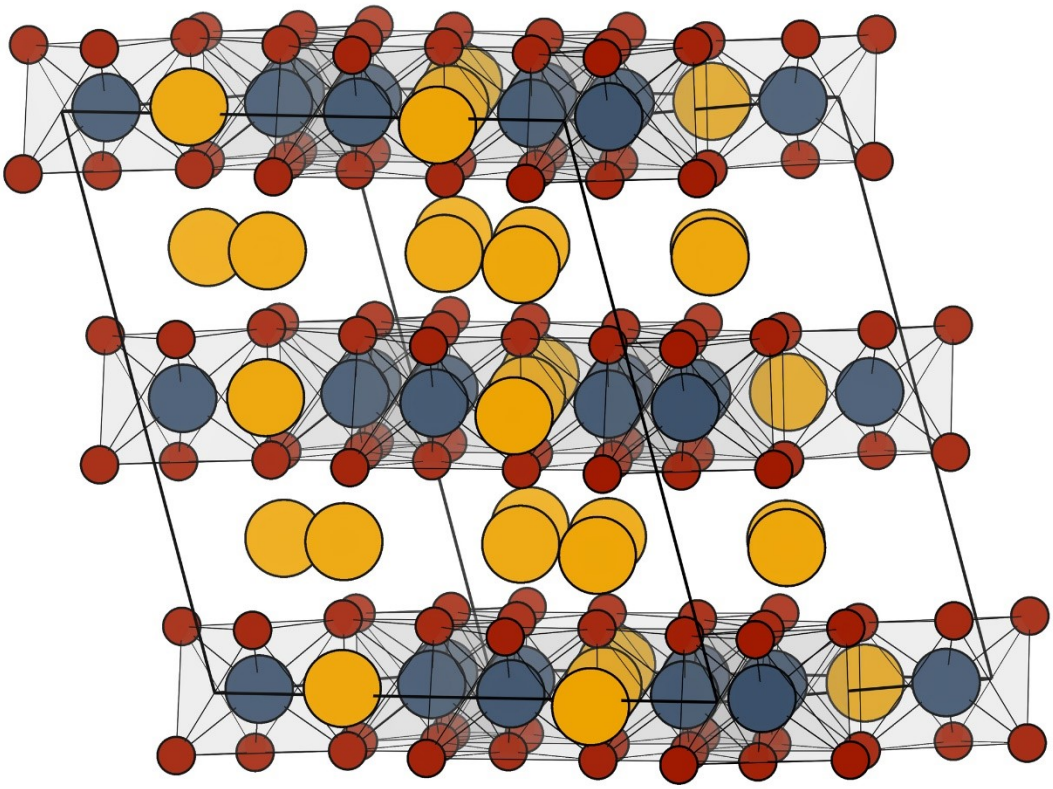

Fig S19 Calculated structure of Li_{14}(Li-layer)Li_6(Mn-layer)$Mn_{16}O_{48}$

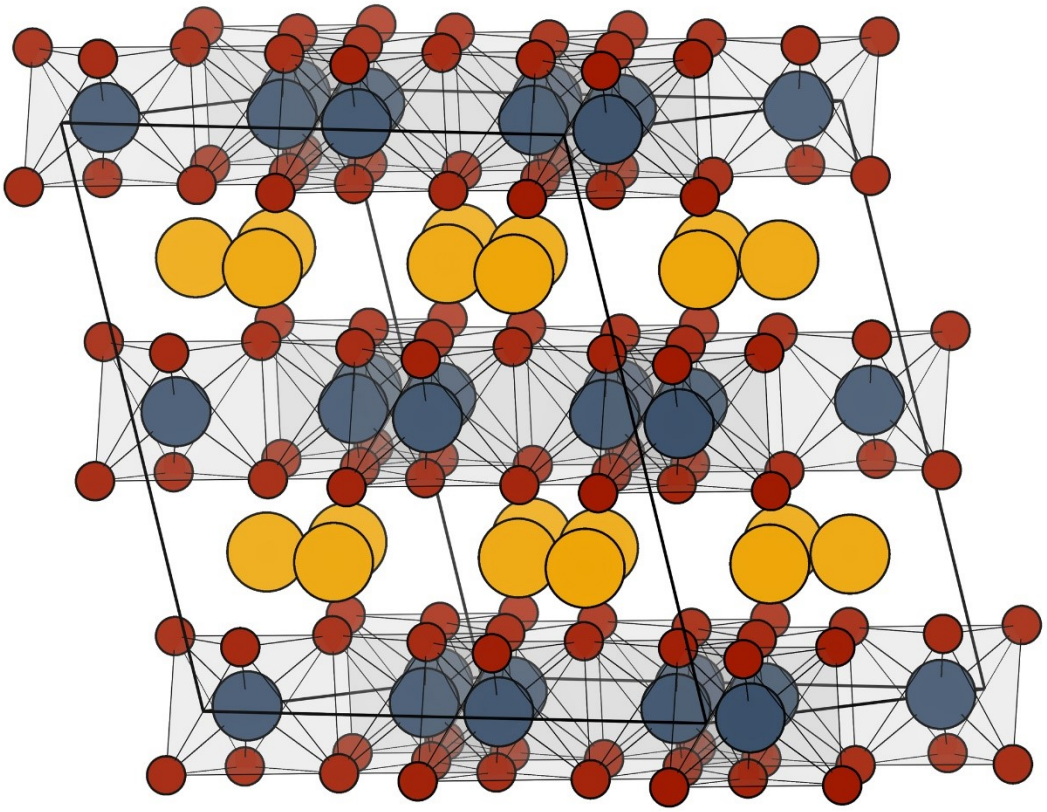

Fig S20 Calculated structure of Li_{16}(Li-layer)Li_0(Mn-layer)$Mn_{16}O_{48}$

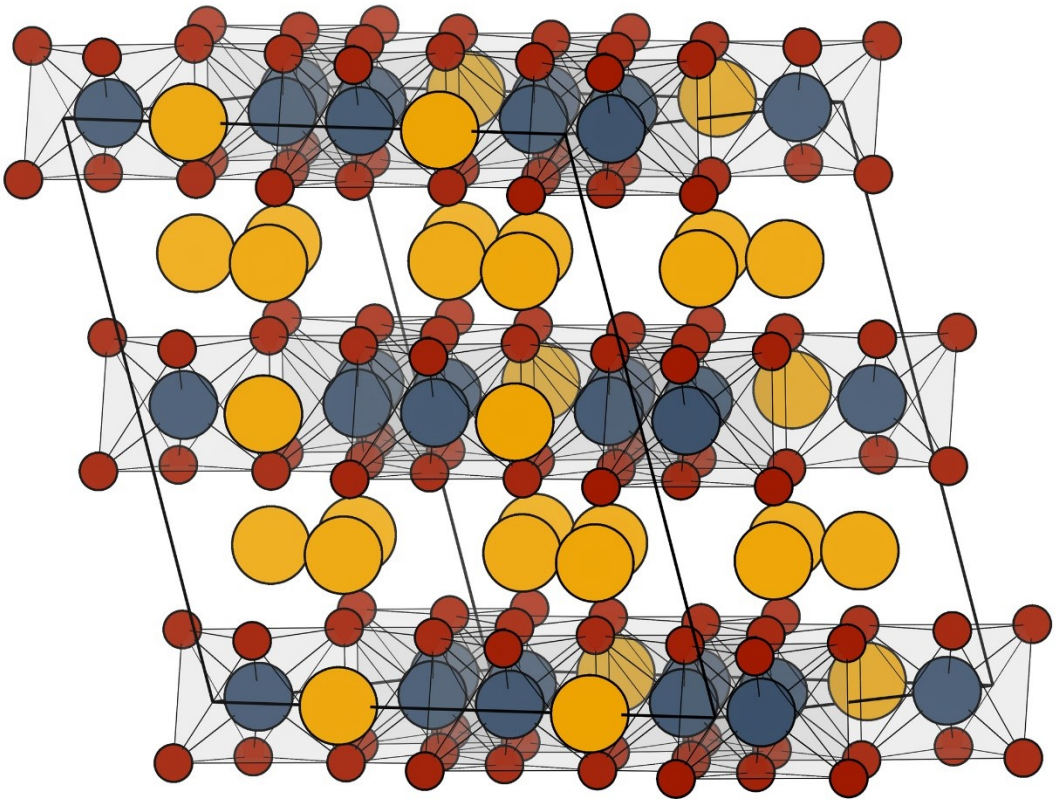

Fig S21 Calculated structure of Li_{16}(Li-layer)Li_4(Mn-layer)$Mn_{16}O_{48}$

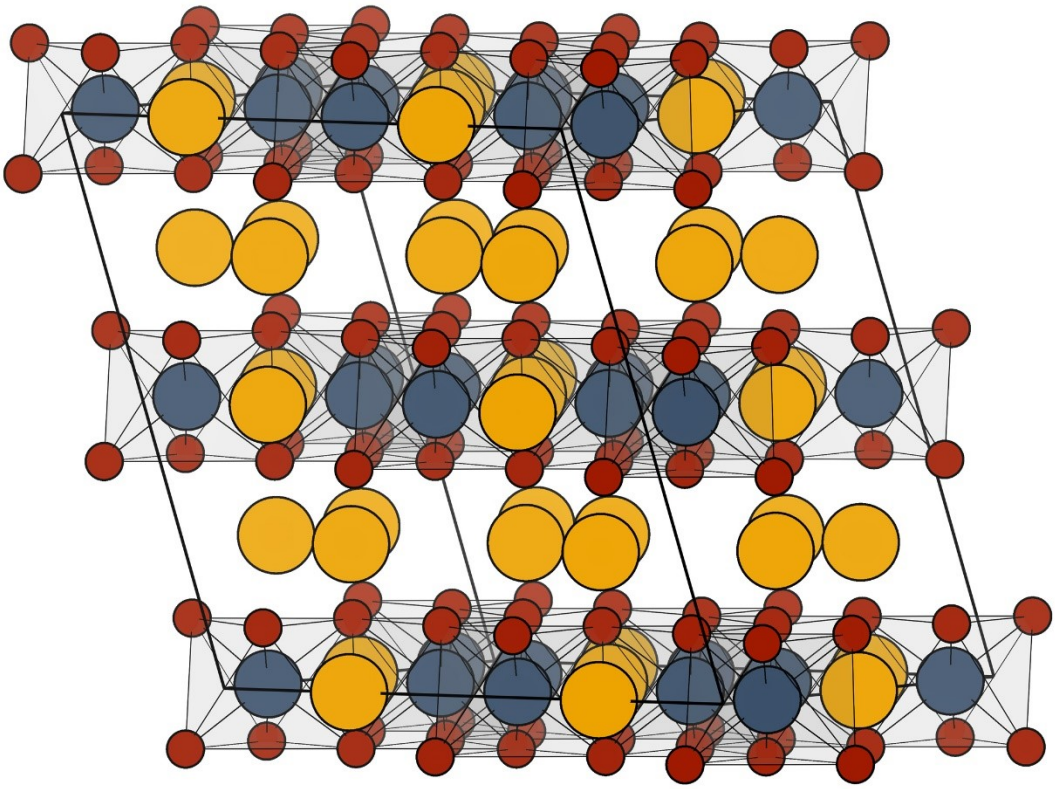

Fig S22 Calculated structure of Li_{16}(Li-layer)Li_8(Mn-layer)$Mn_{16}O_{48}$

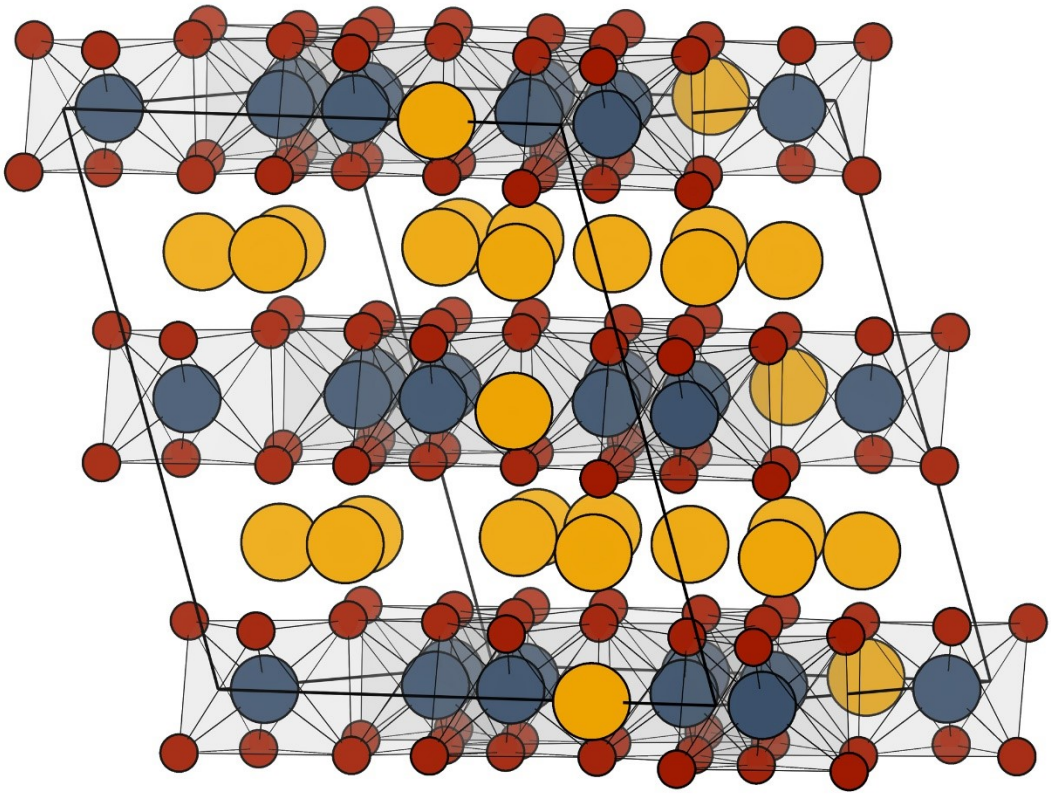

Fig S23 Calculated structure of Li_{18}(Li-layer)Li_2(Mn-layer)$Mn_{16}O_{48}$

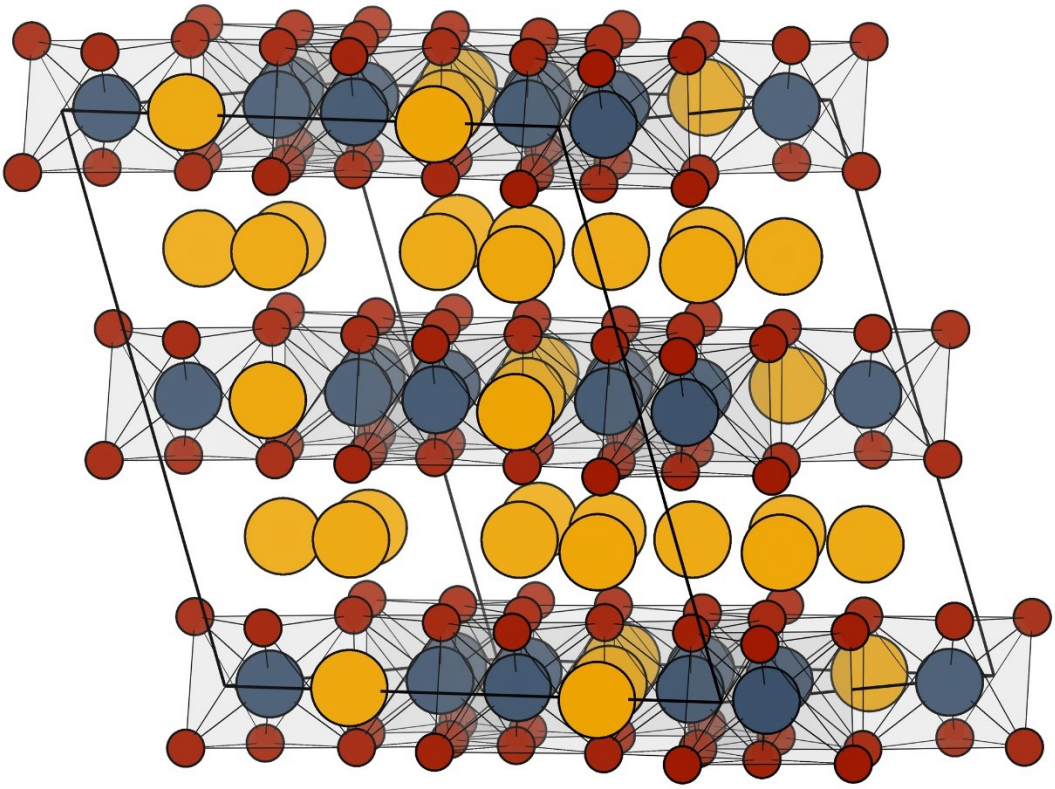

Fig S24 Calculated structure of Li_{18}(Li-layer)Li_6(Mn-layer)$Mn_{16}O_{48}$

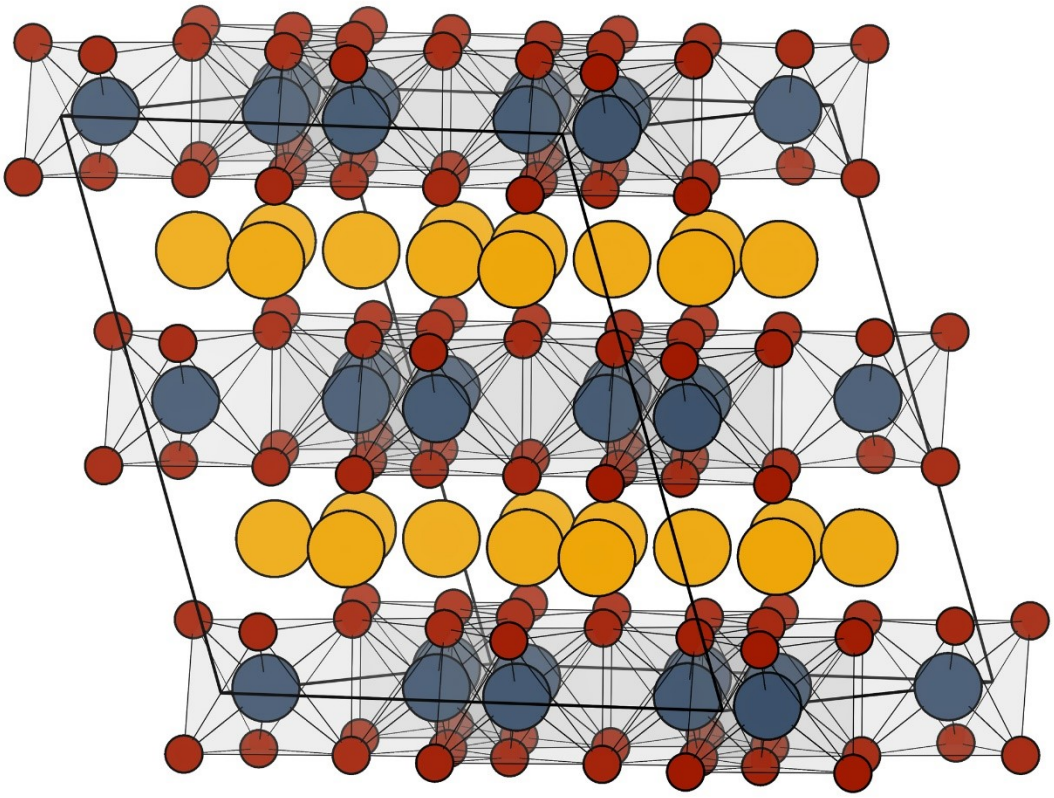

Fig S25 Calculated structure of Li_{20}(Li-layer)Li_0(Mn-layer)$Mn_{16}O_{48}$

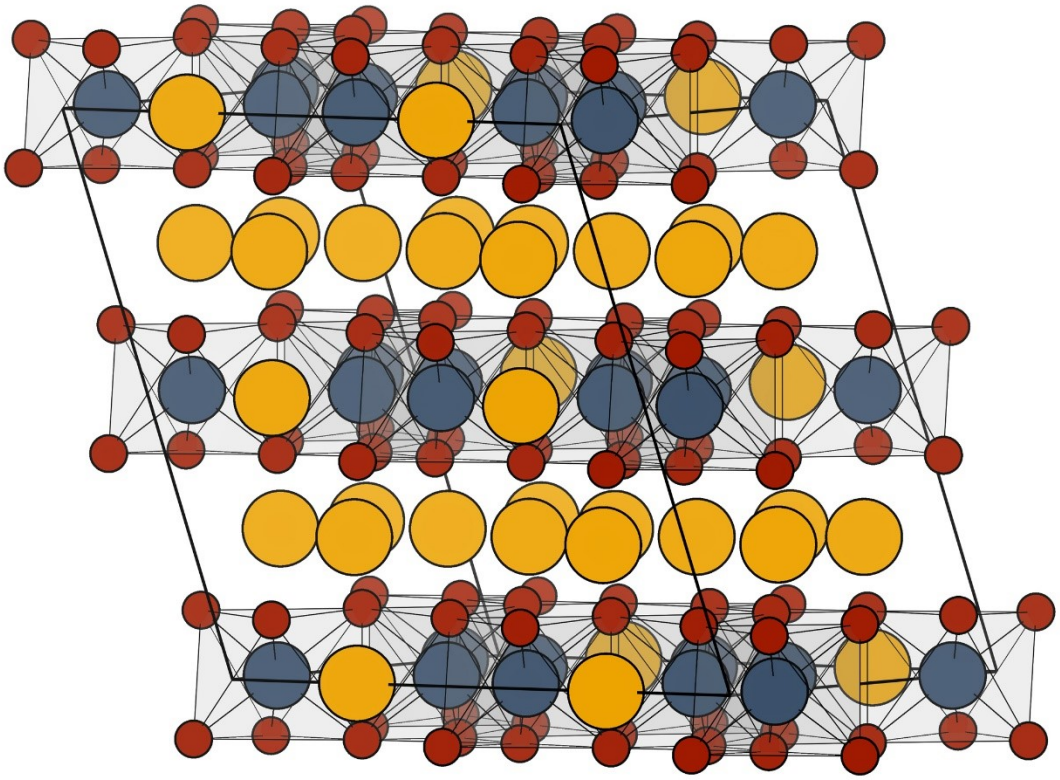

Fig S26 Calculated structure of Li_{20}(Li-layer)Li_4(Mn-layer)$Mn_{16}O_{48}$

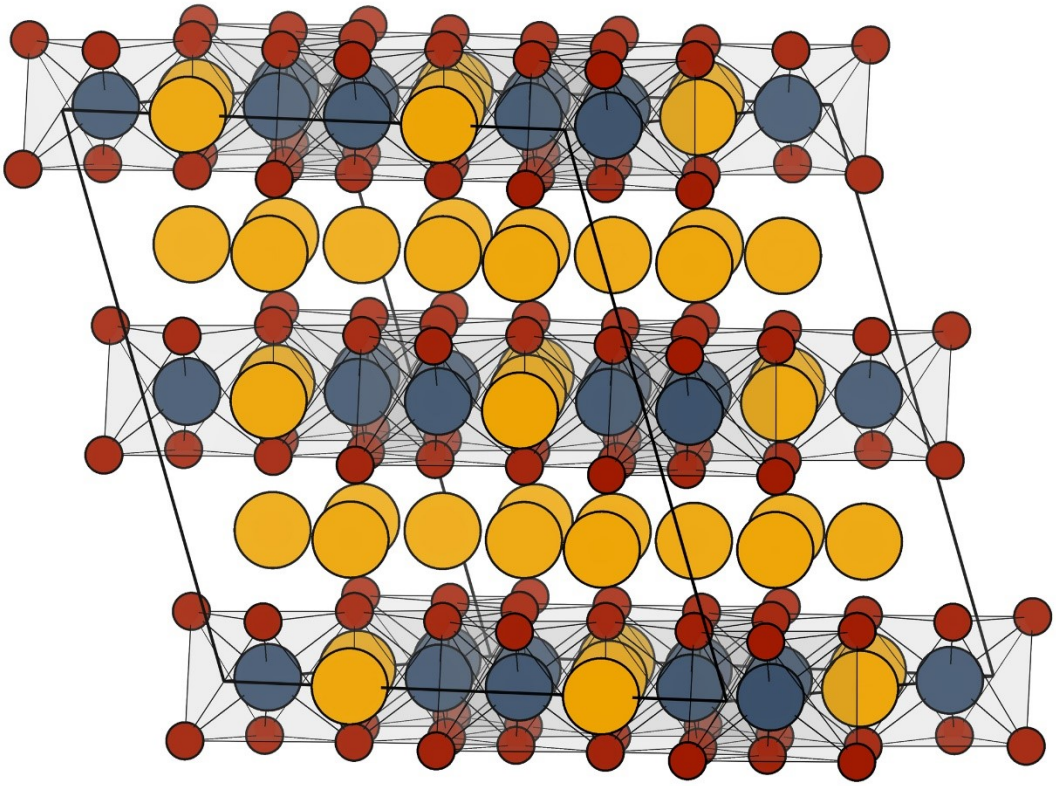

Fig S27 Calculated structure of Li_{20}(Li-layer)Li_8(Mn-layer)$Mn_{16}O_{48}$

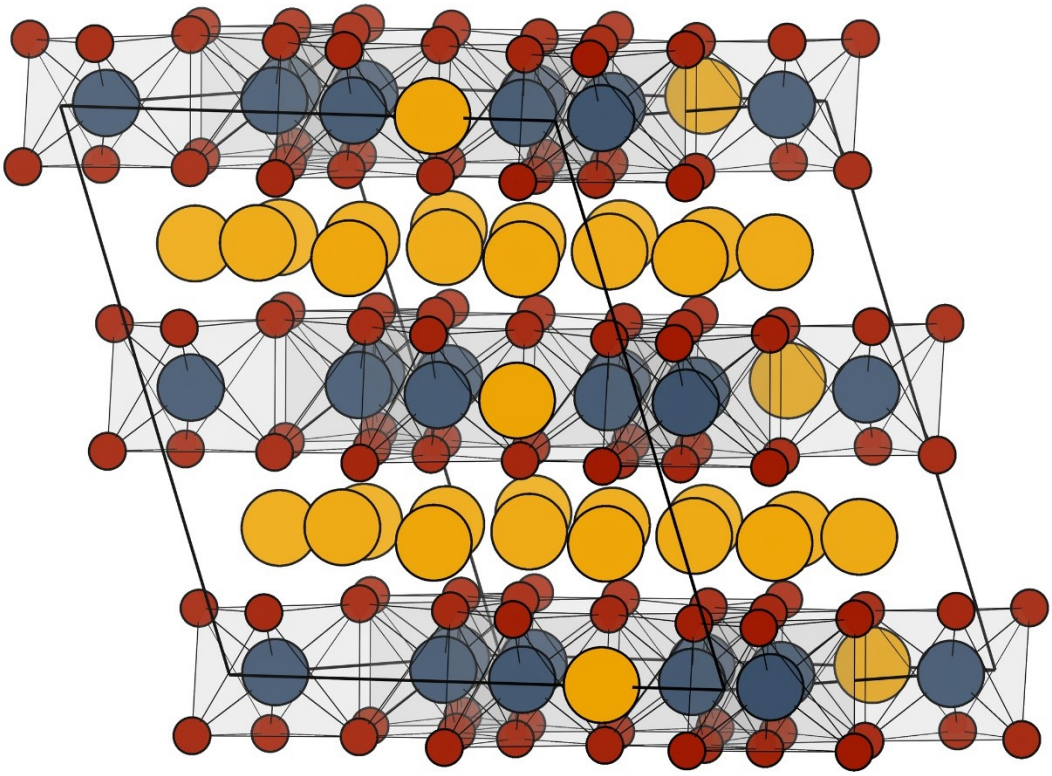

Fig S28 Calculated structure of Li_{22}(Li-layer)Li_2(Mn-layer)$Mn_{16}O_{48}$

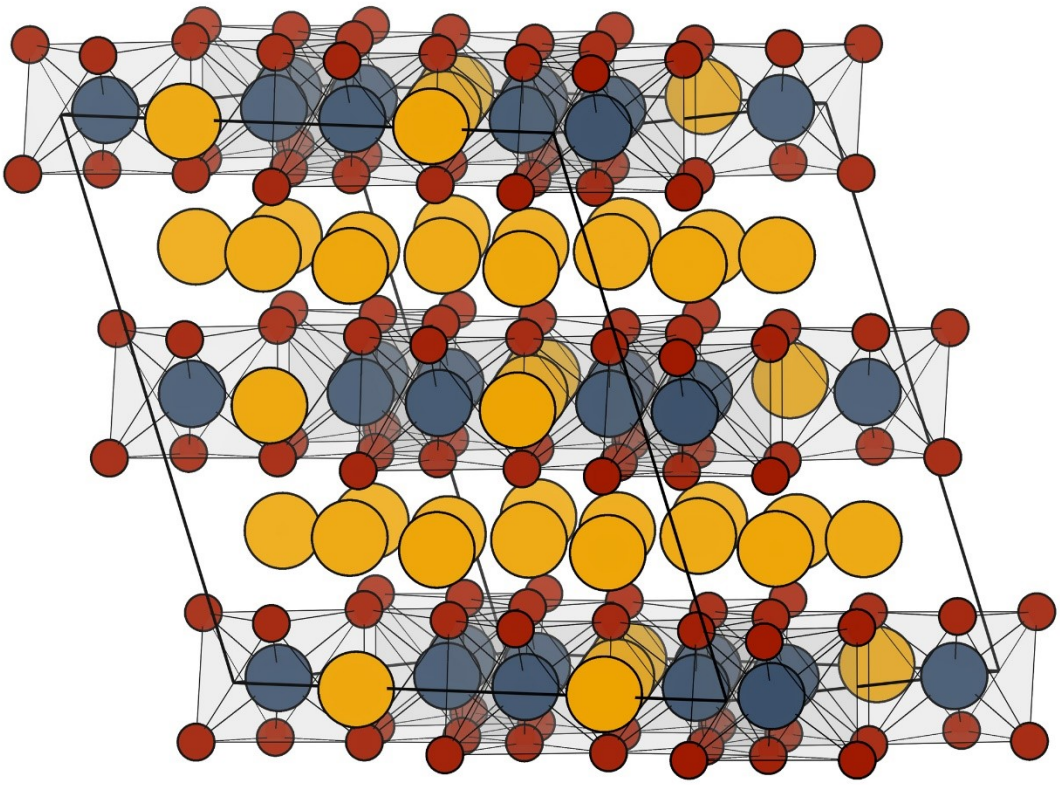

Fig S29 Calculated structure of Li_{22}(Li-layer)Li_6(Mn-layer)$Mn_{16}O_{48}$

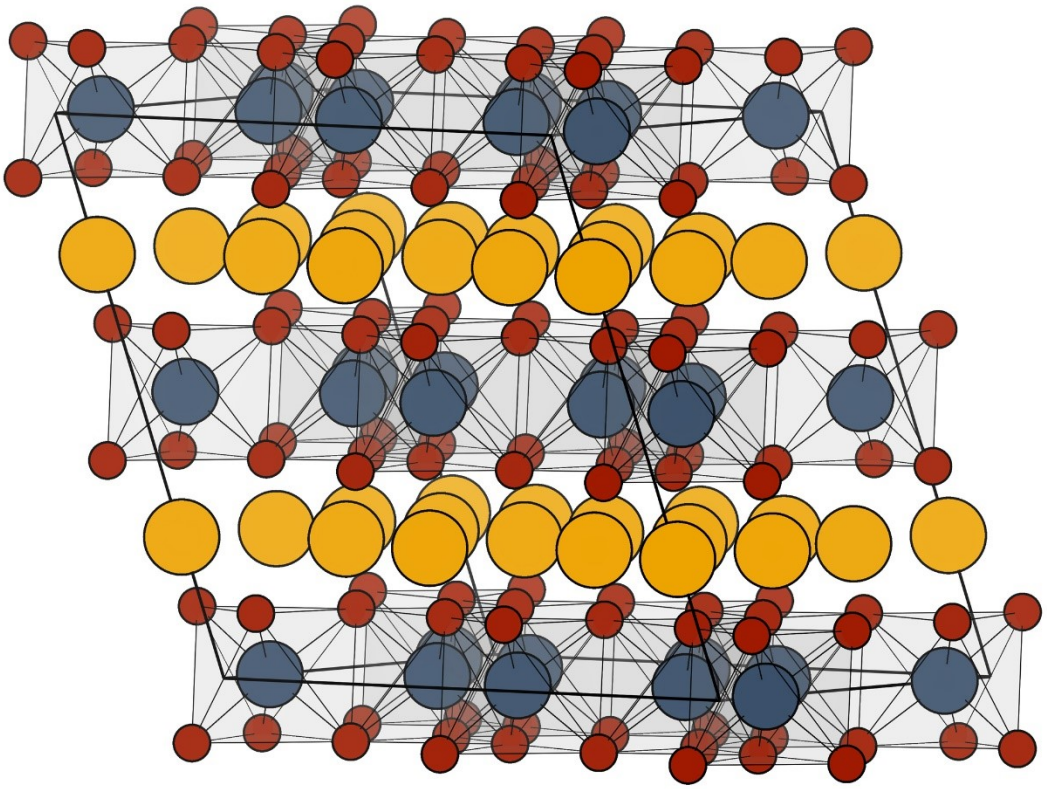

Fig S30 Calculated structure of Li_{24}(Li-layer)Li_0(Mn-layer)$Mn_{16}O_{48}$

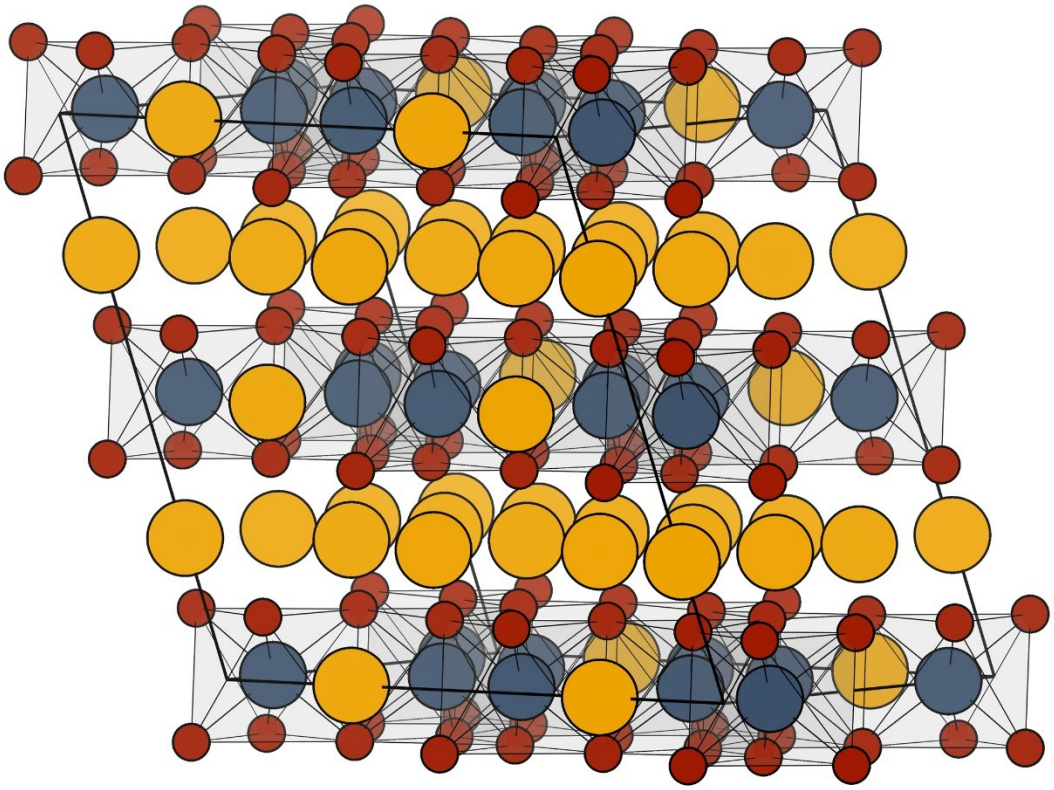

Fig S31 Calculated structure of Li_{24}(Li-layer)Li_4(Mn-layer)$Mn_{16}O_{48}$

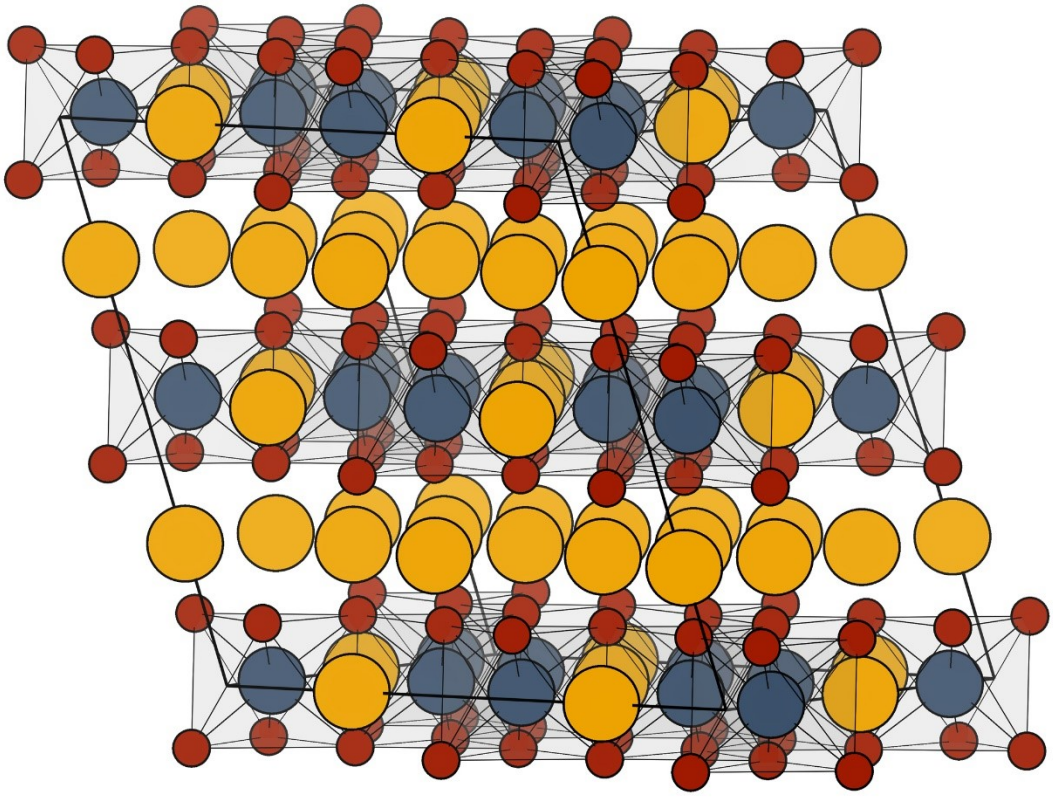

Fig S32 Calculated structure of Li_{24}(Li-layer)Li_8(Mn-layer)$Mn_{16}O_{48}$